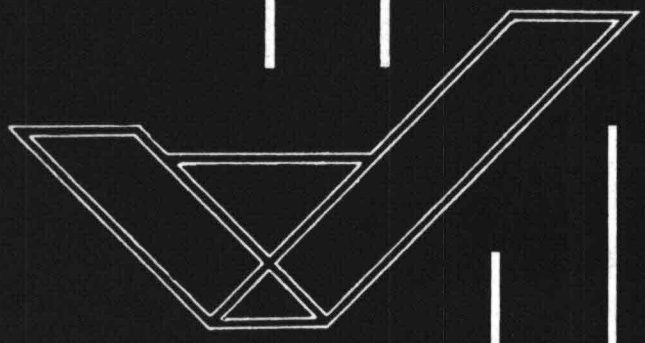

Measurements of turbulent flow in a suddenly expanding flume with a rough bottom

L.X. Wang

Report no. 2-83

Laboratory of Fluid Mechanics
Department of Civil Engineering
Delft University of Technology

MEASUREMENTS OF TURBULENT FLOW IN A SUDDENLY EXPANDING FLUME WITH A ROUGH BOTTOM

L.X. Wang

Water Conservancy and Hydroelectric Power
Research Institute
Beijing, China

Report No. 2 - 83
Laboratory of Fluid Mechanics
Department of Civil Engineering
Delft University of Technology
Delft, The Netherlands

CONTENTS page

Abstract

Some measurements were conducted in a suddenly expanding flume with a rough bottom. In the approach flume, the friction velocity was determined in three ways and the distributions of turbulence intensities and Reynolds stress in a vertical were obtained. The measurement of the separating turbulent flow comprised the distribution of depth-averaged velocity and turbulence quentities (u', v', $-\overline{uv}$ and $\bar{u}^2 + \bar{v}^2$) in the separation region and the vertical distribution of turbulence quentities in the mixing layer. To measure instantaneous velocity components a Laser Doppler Velocimeter and a Data Acquisition System were employed. The data were processed using a digital filter.

Notation

A(i),B(i)	time series of measured data
$\bar{A}$, $\bar{B}$	time averaged values of A(i), B(i)
a(i),b(i)	turbulent fluctuation of A(i), B(i)
a'	$= (\bar{a}^2)^{\frac{1}{2}}$, intensity
B_0	width of the approach flume
B_1	width of the expanding flume
C	Chézy coefficient
C_{cor}	cross correlation coefficient
D	performance of digital filter
d	hydraulic diameter
E,Eu,Ev	turbulence energy
F	focus distance of lens in LDV
Fr	Froude number
Fp	passband cutoff frequency of digital filter
Fs	stopband cutoff frequency of digital filter
ΔF	= Fp - Fs
fc	cutoff frequency of analog filter
fs	sampling frequency of DAS
fi	normalized frequency
g	gravitational acceleration
g(i)	time series of the grating's noise
H(f),H(m)	frequency response of digital filter
h(t),h(n)	impulse reponse or weighting function of digital filter
h	water depth
J	water surface slope
K	ripple ratio of digital filter
k	Nikuradse sand roughness
L	length of a segment for Fast Fourier Transform, except where noted otherwise
M	number of segments in Fast Fourier Transform
N	length of time series of measured data; length of digital filter
P(fi)	power spectrum
Q	discharge
Re	Reynolds number
Tm	measuring time
t	time
U,V,W	instantaneous velocity components

$\bar{U},\bar{V},\bar{W}$	time-averaged velocity components (mean velocities)
u,v,w	turbulent fluctuation of velocity components
u',v',w'	turbulence intensities
U_*	friction velocity
U_0	averaged velocity in a vertical or in a section
x,y,z	cartesian coordinates in three directions
$X(i),X(t)$	output series of digital filter
$x(i),x(t)$	input series of digital filter
δ_1,δ_2	passband ripple and stopband ripple of digital filter
κ	Kármán's universal constant
ρ	density
σ_a^2	variance
τ	time delay or time interval
τ_b	bottom shear stress
τ_w	side-wall shear stress
α	slope of $\bar{U}$-profile on semi-logarithmic scale
λ	nondimensional coefficient of resistance, except where noted otherwise
ν	kinematic viscosity
ϕ	angle

1. Introduction

Many experimental investigations have been done on suddenly expanding (separating) turbulent flows because of their prime importance to understand the separation problem. Several instruments are employed (such as hot wire or hot film anemometers and Laser Doppler Velocimeters) in various experimental set-ups (open channels, ducts, wind tunnels, etc.). This problem is still far from well understood, however. Some results obtained with different measuring techniques, are not in good agreement.

The measurements described here were conducted in a rough-bottom flume with a Laser Doppler Velocimeter (LDV). The flume consisted of a 10 m long, 0.4 m wide approach flume before a sudden expansion and a 5.2 m long, 0.6 m wide expanding flume. Measurements in the expanding flume were concerned with mean velocity and turbulence in the separating flow. In the approach flume the water surface slope, mean velocity and vertical distributions of turbulent quantities were measured. The measured data are to be used for comparison with a numerical model. Attention was also paid to the measuring methods and data processing.

2. Measuring procedure

In this experiment, the same apparatus was employed as in the experiment on unsteady separating flow (ref. 8,17). The flume has two smooth side-walls (perspex) and a rough bottom (sand, median diameter 0.7 mm, glued on glass plates). Two series of measurements were conducted.

The first series of measurements was done in the approach flume, where the water surface slope and the instantaneous velocity components u and w in x- and z-direction were measured in order to determine the bottom shear stress and the vertical distributions of turbulence quantities. The second series was concerned with the instantaneous velocity components u and v in x- and y-direction in the expanding flume. The schemes of the two measurements are shown in fig. 1, in which the origin of coordinates is at the bottom in the expansion section, x-axis takes the flow direction, y- the transverse direction and z- the vertical direction.

2.1 Water-surface slope measurements

The tests in the approach flume were conducted with discharge $Q = 4{,}85 \times 10^{-3}$ m^3/s and water depth h = 6 cm. A small depth was set up in order to get a fully developed turbulent flow. The water surface slopes were determined by measuring the difference in water levels in three cross-sections, using two total-head tubes and transducing in two ways: mechanically and electrically. The cross-sections were 50 cm, 150 cm and 250 cm upstream of the expansion section. In the first way, the water-level difference was projected, with an enlarging factor of 40, onto a screen of a Water-Level Difference Meter (WLDM) and could be read to 0.01 mm. In the second way, the pressure difference was transformed into voltage and displayed digitally by means of a Pressure Transducer (PT) and a Time Domain Analyser (TDA, TYOE JM-1860). Owing to small fluctuation in the flow rate, the signals had to be averaged during a certain time. The averaged reading became stable after a measuring time of 4 to 5 minutes. When using the WLDM, a series of readings was taken sequentially with an interval of 20 seconds and averaged according to

$$\bar{A} = \frac{1}{N} \sum_{i=1}^{N} A(i\Delta t)$$

with Δt = 20 s and $N\Delta t$ = 300 s. In the second case, the integration was carried out analogically by the instrument, also for a period of 5 minutes. Because of the inaccuracy of manufacturing of the total-head tubes, the systematic error of the measurement was too large. It can be easily eliminated, however, by interchanging the positions of the tubes, testing twice and taking the mean value of the readings. The test was repeated two or three times and the readings were averaged.

2.2 Velocity measurements in the approach flume

The measurements of U and W in the approach flume were done in three verticals b, c and d in section I (x = 72 cm, y = 12, 20 and 28 cm) and at five points in each vertical. The same LDV (TPD - 1077/2M) was employed as in the previous investigation (ref. 8, 17), but the laser beams were set up horizontally instead of vertically in order to measure the x- and z-components of the velocity. A long-focus lens (F = 600 mm) was used for the measurements in the 0.4 m wide flume. The angle between the two laser beams (in air) is $\phi = 2.826^{\circ}$. The sizes of the measuring volume are:

width $bx = 4 \lambda F/\pi\, bo \cos(\phi/2) = 0.48$ mm,

length $by = N_r bx/\tan(\phi/2) = 26.04$ mm,

where λ = laser light wavelength = 632.8 mm, b_0 = ($1/e^2$ intensity limited) diameter of the laser beam = 1 mm and N_r = reflective index of water = 1.33.

For measuring mean velocities, the TDA was connected with the frequency tracker and the time-integrated signals $\bar{A}$ were shown by the digital display, according to

$$\bar{A} = \frac{1}{T} \int_0^T A(t)dt$$

with integration time T = 3 to 5 minutes for each measurement. The measurement was done wtice at each point and then the mean value was taken. The theoretical relation between tracker output (voltage) and flow velocity is:

1 mv = 0,25662 cm/s

To obtain instantaneous velocities the signals were sampled, transmitted by the Data Acquisition System (DAS) and recorded on a magnetic tape for subsequent data processing. In order to fully utilize the recording range of DAS, different values of amplifying factors were selected for the components recorded. In fig. 2, a block-scheme of the transformation from flow velocity to digitized signals of DAS is given. The calibration factors are as follows:

in channel 1, for measuring U, 1 level = 0.31328×10^{-2} cm/s,

in channel 2, for measuring W, 1 level = 0.15664×10^{-2} cm/s.

2.3. Velocity measurements in the expanding flume

In the measurement of the separating flow, a discharge of $Q = 20 \times 10^{-3}$ m^3/s was supplied to the flume (fig. 1); the water depth varied from 9.05 cm to 9.65 cm along the flume. The LDV was set up vertically and the two horizontal components of the velocity were measured at 31 verticals. Three measuring points were taken in each vertical. In the mixing layer five points in each vertical were taken in order to get the vertical distributions. The sand glued onto the glass bottom was removed at the measuring positions. The focus distance of the front lens of the LDV was F = 242.5 mm. In this case, the sizes of the measuring volume are: angle $\phi = 6.985^{o}$, width bx = 0.20 mm and length by = 4.27 mm.. The calibration factors are:

in channel 1, for measuring U, 1 level = 0.63406×10^{-2} cm/s,

in channel 2, for measuring V, 1 level = 0.31703×10^{-2} cm/s.

2.4 Sampling frequency and particle seeding

The sampling frequency fs is two times the cutoff frequency (f_c, Nyquist frequency) of the lowpass filter (fig. 2). f_c should be high enough to cover the range containing the major part of the frequencies contributing to the Reynolds stress. In the first series of measurements (in the approach flume) f_c = 50 Hz was selected. It has been found by means of spectral analysis on the computer that this value of f_c is so high that the sampled data contain a noise caused by the inconstant speed of the rotating grating, which is used to preshift the frequency of the laser beams. The energy spectrum of the noise has a peak at a frequency of about 48 Hz. However, the dominating turbulences (energy-containing eddies) have frequencies

under 25 Hz. In the measurements of separating flow,spectral estimates were made on the Correlator (HP Model 3721 A and 3720 A) with different cutoff frequencies, namely 15, 25 and 35 Hz. The energy spectra are almost the same when fc = 25 Hz and 35 Hz, but some information is lost when fc = 15 Hz. In order to filter out the 48 Hz noise, to get sufficient information and to create shorter data series, the cut-off frequency in the second measurement was set equal to 25 Hz.

In the second series of measurements the water in the supply system was so clean that there were not enough particles to reflect the laser beams. The presence of the frequency tracker was as low as 25%. It is difficult to improve the presence by seeding particles because the system is very large. In order to see the influence of a low presence, a comparative test was conducted. By seeding particles temporarilly at the entrance of the flume, the presence could reach 35%. The spectrum then obtained showed no difference from that in the case of 25% presence.

3. Data processing

3.1 Calculation formulae

In the velocity measurements, two time series A(i) and B(i) were simultaneously obtained by sampling two components in x- and z- or in x- and y-directions with frequency fs. To calculate time-averaged and turbulent quantities of a steady flow, the following formulae were used:

(1), for the mean value $\bar{A}$ and the turbulent fluctuation a(i),

$$\bar{A} = \frac{1}{N} \sum_{i=1}^{N} A(i)$$

$$a(i) = A(i) - \bar{A} \qquad (1)$$

(2), for the variance σ_a^2 and the turbulence intensity a',

$$\sigma_a^2 = \frac{1}{N} \sum_{i=1}^{N} a^2(i) \qquad (2)$$

$$a' = \sqrt{\sigma_a^2}$$

(3), for the cross product (Reynolds stress),

$$-\overline{ab} = -\frac{1}{N} \sum_{i=1}^{N} a(i)\, b(i) \qquad (3)$$

(4), for the quantity E, designated here as the turbulence energy (although it differs somewhat from the correct definition of turbulence energy),

$$E = \sigma_a^2 + \sigma_b^2$$

where N = fs x Tm is the length of the series A(i) and B(i), and Tm is the measuring time. The results of the computations should be independent of N when Tm is sufficiently large. A comparison was made between the results when Tm = 180, 240 and 300 s, which showed that Tm = 180 s was not sufficient and small differences (= 2 to 4%) were obtained between the results when Tm = 240 s and 300 s. The measuring time Tm = 270 s was selected in the first series of measurements (with fs = 100 Hz) and Tm = 300 s (with f_s = 50 s) in the second series.

3.2 Power-spectral estimates

In the first series of measurements, f_s = 100 Hz was selected. Owing to the noise mentioned, the calculated results according to the formulae listed above were not correct. In order to examine the noise, power spectral estimates were made at two measuring points. The standard subroutine FTFPS in the IMSL Library was used.

In this subroutine, the serires of sampled signals is divided into segments, each of which has a length L (L is a power of 2). The length of the series is N = M x L; $M \geq 15$ is recommended. To each segment, the Fast Fourier Transform (FFT) is given by FTFPS with a triangular window, from which spectral estimates are calculated for that segment, and all the estimates of the M segments are averaged to obtain the spectral estimate.

The output $P(f_i) = \frac{1}{2} \times f_s \times E(f_i)$ is given at the following normalized (with f_s) frequencies

$$f_i = \frac{i-1}{L}, \quad i = 1, 2, \ldots\ldots, \frac{L}{2} + 1$$

Non-dimensional power-spectra, i.e, $f_s\, Eu/(2u'^2)$ and $f_s\, Ew/(2w'^2)$, of the U and W components at point b3 (x = 72 cm, y = 28 cm, z = 2.7 cm) are depicted in fig. 3, with L = 128, M = 200 and f_s = 100 Hz. It can be seen that a strong noise exists around 48 Hz. The energy peaks in both components are high and narrow, and so it is easy to use a digital filter to filter out the noise.

3.3 Digital filtering

A digital filter is essentially an algorithm for signal processing that selects frequencies by transmitting a certain range (or ranges) of frequencies and rejects others. It can be realized by programming a digital computer, which is fed with a time series x(i) or x(t), where $t = i\Delta t$. The output is a convolution integral of x(t).

$$X(t) = \int_{-\infty}^{\infty} h(\tau)\, x(t - \tau)\, d\tau$$

or, in discrete form,

$$X(i) = \sum_{n=-\infty}^{\infty} h(n)\, x(i - n)$$

where $h(\tau)$ or/and $h(n)$ is the weighting function of the filter. $h(n)$ is also designated as impulse response function or filter coefficients.

The frequency response function of the filter $H(f)$, or $H(m)$, is the Fourier transform of $h(\tau)$, or $h(n)$, defined by

$$H(f) = \int_{-\infty}^{\infty} h(\tau) e^{-i2\pi f\tau} d\tau$$

or $$H(m) = H(e^{i2\pi m}) = \sum_{n=-\infty}^{\infty} h(n) e^{-i2\pi mn}$$

The structure of filters used shows a great variety. For this investigation, a lowpass FIR filter (Finite Impulse Response digital filter) was selected by adopting a standard program given in ref.(13). For a lowpass filter the optimal design problem consists of specifying the filter length N, the passband cutoff frequency Fp, the stepband cutoff frequency Fs (Fp and Fs normalized with fs), and the ripple ratio $K = \sigma_1/\sigma_2$, where σ_1 is the passband ripple and σ_2 the stopband ripple. The width of the transition band of the filter is $\Delta F = Fs - Fp$. Fig. 4 shows the frequency response of a lowpass filter.

The FIR Design Program on page 194 of ref. (13) produces a linear phase FIR filter of symmetrical form, using Remes exchange algorithm, with an odd number N of filter length ($3 \leq N \leq 256$). Up to 10 frequency-regions, defined with Fp and Fs, can be specified within f = 0 to 0,5. This program gives the filter coefficients $h(n)$, n = 1, 2 ....N and the ripples σ_1 and σ_2, which are the maximum deviations of $H(m)$ from 1 and 0 in passband and stopband respectively. A general problem is that the deviations become larger if the specified ΔF is smaller. The program minimizes the ripples for a given ΔF. Another compromise has to be made between N and F, K and σ_2. Generally, for a given K, the longer N is, the better is the property of the filter and the more computing time is needed. For an optimal Chebyshev lowpass filter, the performance, defined as $D = (N - 1)\Delta F$, is essentially independent of N, if $N \geq 51$.

After the filter coefficients h(n) have been obtained, the time series x(i) is smoothed according to

$$\sum_{n=0}^{N} h(n)\ x(i-1+n) = X(i)$$

In this investigation the following values were assumed: N = 51, Fp = 0.3, Fs = 0.45 and K = 1. The program then gave

$$\sigma_1 = \sigma_2 = 0.396 \times 10^{-6}$$

and h(n), n = 1, 2 .....N
In this case the deviation at F = 0 is positive, therefore the filtered series X(i) is shifted upwards by σ_1 and should be corrected with

$$X_{corr}(i) = \frac{1}{1+\sigma_1} X(i)$$

3.4 Step-shifting calculation

A simple way to eliminate the 48 Hz noise is the step-shifting method, which can be used here since f_s is about two times the frequency of the noise. For calculating turbulence quantities, in addition to the formulae (1), (2) and (3), the following expressions are also applied:

$$(\sigma_a^2)_1 = \frac{1}{N} \sum_{i=1}^{N} a(i)\ a(i+1) \qquad (4)$$

$$(-\overline{ab})_1 = -\frac{1}{N} \sum_{i=1}^{N} a(i)\ b(i+1) \qquad (5)$$

The sampled signal $a(i) = A(i) - \bar{A}$ consists of two parts: the turbulent fluctuation of the flow $a_t(i)$ and the grating's noise g(i). It is assumed that the noise may be written as a sum of sine functions of time.

$$g(i) = \Sigma \hat{g}_k \sin 2\pi f_k t$$

$$= \Sigma \hat{g}_k \sin 2\pi k f_0 t$$

where $k = 1,2 \ldots,$ $t = i\Delta t$, Δt = sampling interval and $f_s = 48$ Hz. When the cutoff frequency of the lowpass filter of the tracker $f_c = 50$ Hz, only the first component with

$f_1 = 48$ Hz of the noise has been sampled. For $\Delta t = 1/f_s = 1/100$ s,

$$g(i) = \hat{g} \sin(2\pi \times \frac{48}{100} i)$$

since $f_0 \simeq f_c$,

$$g(i+1) = \hat{g} \sin(2\pi \times \frac{48}{100} i + \frac{48}{50}\pi)$$

$$\simeq - g(i)$$

So, for the sampled signals, we have

$$a(i) = a_t(i) + g(i)$$

$$a(i+1) = a_t(i+1) - g(i)$$

By using expression (4),

$$(\sigma_a^2)_1 = \frac{1}{N}\left[\Sigma a_t(i)a_t(i+1) + \Sigma a_t(i)\, g(i+1) + \Sigma a_t(i+1)g(i) - \Sigma g^2(i)\right]$$

The auto-correlation function of flow turbulence is

$$R_{11}(\tau) = \frac{\overline{a_t(t)\; a_t(t+\tau)}}{\overline{a_t^2(t)}}$$

when $\tau \to 0$, $R_{11}(\tau) = 1$. In this case, for shifting by one step, $\tau = \Delta t = 1/100$ s, and $R_{11}(\tau) \simeq 1$, so

$$\Sigma a_t(i)\; a_t(i+1) \simeq \Sigma a^2(i)$$

Also, $a_t(i)$ is a random series independent of $g(i)$, so that the cross correlation of $a_t(i)$ and $g(i)$ should be equal to zero. So we have

$$(\sigma_a^2)_1 = \frac{1}{N} \sum_{i=1}^{N} a(i)\; a(i+1)$$

$$\simeq \frac{1}{N} \sum_{i=1}^{N} \left[a_t^2(i) - g^2(i)\right]$$

if we set

$$(\sigma_a^2)_0 = \frac{1}{N} \sum_{i=1}^{N} a^2(i)$$

$$\simeq \frac{1}{N} \sum_{i=1}^{N} \left[a_t^2(i) + g^2(i)\right]$$

then the variance of the turbulence is

$$\sigma_a^2 = \sum_{i=1}^{N} a_t^2(i) = \frac{1}{2}\left[(\sigma_a^2)_1 + (\sigma_a^2)_0\right]$$

The same procedure can be applied to the cross product of the two components for which we have

$$(-\overline{ab})_0 = -\frac{1}{N} \sum_{i=1}^{N} a(i)\, b(i) = \frac{1}{N}\left[-\sum_{i=1}^{N} a_t(i)\, b_t(i) - \sum_{i=1}^{N} g^2(i)\right]$$

$$(-\overline{ab})_1 = -\frac{1}{N} \sum_{i=1}^{N} a(i)\, b(i+1) = \frac{1}{N}\left[-\sum_{i=1}^{N} a_t(i)\, b_t(i) + \sum_{i=1}^{N} g^2(i)\right]$$

so that the Reynolds stress becomes

$$-\overline{ab} = -\sum_{i=1}^{N} a_t(i)\, b_t(i) = \frac{1}{2}\left[(-\overline{ab})_1 + (-\overline{ab})_0\right]$$

Furthermore, if we set the following approximation,

$$g(i+2) \simeq -g(i+1) \simeq g(i)$$

then, $(\sigma_a^2)_2 = \frac{1}{N} \Sigma a(i)\, a(i+2)$

$$\simeq \frac{1}{N} \Sigma\left[a_t^2(i) + g^2(i)\right]$$

$$\simeq (\sigma_a^2)_0$$

and also $(\sigma_a^2)_3 \simeq (\sigma_a^2)_1$

In fig. 4 it can be seen that turbulence quantities calculated according to the expression

$$(\sigma_a^2)_j = \frac{1}{N} \sum_{i=1}^{N} a(i)\, a(i+j)$$

oscillate with shifted steps j(j=0, ±1, ±2, ±3), as predicted.

The step-shifting calculation is essentially a procedure of filtering. A comparison was made between the two methods: step-shifting calculation and digital filtering in processing the data in vertical C. In this particular case, the results of the two calculations are almost the same. The differences between the two calculations are less than 1% for time-averaged velocities $\bar{U}$ and $\bar{W}$, and less than 5% for turbulence quantities u', w', $-\overline{uw}$ and $(\bar{u}^2 + \bar{w}^2)$. The final results presented in this report were obtained with the step-shifting calculation.

3.5 A brief description of the programs

The sampled data recorded on the magnetic tapes have to be converted and reorganized before they can be read for compution. A number of programs has been compiled for data processing on the computer. A brief description of the programs is given below.

MAIN PROGRAM declares the dimensions of arrays; gives parameters such as sampling frequency, measuring time, calibration factors, etc.; calls desired subroutines and writes the final results of computation.

SUBPROGRAMS:

W1RDDT reads sampled data from the working tapes into two one-dimensional arrays for further computation by calling a standard subroutine READR1, ref.(18);

W2TURB calculates the mean values and two series of fluctuating values; calculates the cross-product of two series and calculates variances of the two series;

W5RSLT calculates mean velocities, turbulence intensities, Reynolds stresses and turbulence energy, using calibration factors;

W8SPES calculates spectral estimates by calling a standard subroutine FTFPS (in the IMSL Library);

FILTER. JCL specifies the parameters of the filter which is to be designed; calls subroutine FILTER. FOR;

FILTER.FOR calculates the filter coefficients, which is essentially the standard program in ref. (13);

SMO filters the two series digitally with the filter coefficients.

In the computations different combinations of subroutines are employed for different purposes.

4. Results of measurements

4.1 Measurements in the approach flume

4.1.1 Friction velocity

The bottom shear stresses were determined in three ways: by means of the measured water surface slope, the vertical velocity-profiles and the distribution of the Reynolds stress in the vertical.

Firstly, for a gradually varied flow with a horizontal bottom, the equation of motion reads

$$\frac{dh}{dx} + \frac{d}{dx}\left(\frac{U_0^2}{2g}\right) = -\frac{1}{\rho g h}\left(\tau_b + \frac{2h}{B_0}\tau_w\right)$$

where $U_0 = \frac{Q}{B_0 h}$, the averaged velocity in a section

$\tau_b = \rho U_*^2$, bottom shear stress,

$\tau_w = \frac{1}{8}\lambda\,\rho U_0^2$, side-wall shear stress.

For the fully developed turbulent flow with smooth side walls, the Blasius formula is used to calculate the resistance coefficient λ of the side walls, ref.(19)

$$\lambda = \frac{0.3164}{Re^{\frac{1}{4}}}$$

where the Reynolds number $Re = 4\,U_0 d/\nu$ and the hydraulic diameter $d = B_0 h/(B_0+2h)$. Then, for solving the friction velocity U_*, we have

$$U_*^2 = -gh(1 - Fr^2)\frac{dh}{dx} - \frac{h}{B_0}\cdot\frac{\lambda}{4}U_0^2 \qquad (6)$$

where the Froude number $Fr = U_0/(gh)^{\frac{1}{2}}$.

In this measurement, $Q = 4850\ cm^3/s$, $B_0 = 40$ cm and $h = 6$ cm, we have $Re = 3.7 \times 10^4$, $Fr = 0.263$ and

$$U_*^2 = 0.55 \times 10^4 \times J - 0.35 \quad (cm^2/s^2)$$

where $J = -\frac{dh}{dx} = \frac{\Delta h}{\Delta X}$

The difference Δh in water level between two testing sections were measured with WLDM, or with a Pressure Transducer (PT). The results of the two tests and the calculated bottom friction velocity U_* are presented in Table 1.

Section II was very close to the expansion section, so the water level in section II may have been influenced by the expansion. To calculate the friction velocity in the approach flume, the water level difference Δh between sections III and IV should be taken. Averaging the results measured with WLDM and PT, $U_* = 1.49$ cm/s is obtained.

Secondly, for the fully developed turbulent flow, the velocity profile has a logarithmic form.

$$\bar{U} = \frac{U_*}{\kappa} \ln \frac{z}{k} + c'$$

According to the measured data, we can draw a velocity profile which may be expressed as follows

$$\bar{U} = \alpha U_0 \ln \frac{z}{k} + c'$$

where $\bar{U}$ is the time-averaged velocity measured with LDV and TDA or with LDV and DAS; U_0 is a reference velocity here assumed to be 20 cm/s; k = Nikuradse roughness = 0.07 cm (median diameter of sand glued on the glass bottom); $\kappa = 0.4$; z = the height of measuring points above the bottom; α = slope of $\bar{U}$-profile on semi-logarithmic scale and c' is a constant. Comparing the two expressions, U_* can be calculated from

$$U_* = \kappa \alpha U_0$$

The $\bar{U}$-profiles in three verticals b, c and d are depicted in fig.6 on semi-logarithmic scales. The slope α and calculated U_* are presented in Table 2. Averaging the results gives $U_* = 1.43$ cm/s.

Thirdly, the friction velocity was determined from the distribution of the Reynolds stress. In fully developed turbulent flow in open channels, the Reynolds stress is linearly distributed along a vertical. Extrapolating this distribution to the bottom, U_* can be found from

$$U_*^2 = (-\overline{uw})_{z=0}$$

In this way, U_* is found to be about 1.0 cm/s, see fig. 8 and the next section for comment on the observed nonlinear distribution of the Reynolds stress.

The values of U_* obtained in the above three ways, are listed in Table 3. The differences between the results are rather large. Among these values, the one obtained from the water surface slope is in good agreement with the one obtained with LDV and TDA. Its corresponding Chézy coefficient = 42 $m^{\frac{1}{2}}/s$. The last value of U_* (= 1.0 cm/s) in Table 3 is not reliable because of the inaccuracy of the measurement of the Reynolds stress, see the next section.

To estimate the value of the Chézy Coefficient C, the Colebrook-White formula for the transition region of flow (because $4 < U_* k/\nu = 10 < 100$) in open channels is used, see ref. (20),

$$\frac{C}{\sqrt{8g}} = -2 \log_{10}\left(\frac{k}{12d} + \frac{2.5}{Re\sqrt{fr}}\right)$$

in which

$$\frac{1}{\sqrt{fr}} = \frac{C}{\sqrt{8g}}$$

In this case, the estimated value of C = 49 $m^{\frac{1}{2}}/s$ is obtained.

4.1.2 Vertical distribution of turbulence quantities

Many measurements of turbulence quatities in boundary layers and in pipe flow have been made, ref. 16. The results of this experiment, including the vertical distributions of u'/U_0, w'/U_0 and $-\overline{uw}$, are shown in fig. 7; here U_0 is the depth-averaged velocity. The Reynolds number $Re = U_0 h/\nu$ of the flow was about 1.2×10^4. As far as the relative turbulence intensities u'/U_0 and w'/U_0 are concerned, the distributions are similar to that in pipe flow (ref. 6, fig. 7-56), except that here is a drop of u'/U_0 and w'/U_0 in the lower part of the flow. This drop is larger in the Reynolds stress distribution.

The drop of turbulence quantities in the lower part of the flow is anomalous. A possible source of errors is the large size of the measuring volume of the LDV system (0.48 mm wide and 26 mm long) and the relatively small sizes of vortices near the bottom. In this case, signals recieved by the photodetectors may be related to several vortices moving in different directions.

From the results, a few conclusions can be drawn:

a. Ignoring the drop near the bottom, the distribution of the Reynolds stress in the upper part of the flow shows a linear tendency. According to this tendency, $-\overline{uw}$ reaches a value of about 1.0 cm^2/s^2 at the bottom.

b. Contrary to the Reynolds stress and the turbulence intensities, the cross-correlation coefficient $C_{cor} = (-\overline{uw})/u'w'$ does not show a drop near the bottom. It is 0.30 to 0.41 at $z/h = 0.15$ to 0.65, which is in the same range as found by other workers. For pipe flow, C_{cor} is 0.37 to 0.45. At $z = 0.85$ h, C_{cor} = 0.15 to 0.30 in this experiment and $C_{cor} = 0.21$ in pipe flow, (ref. 6).

c. The sampling frequency was not very high. Some information at higher frequencies was lost, which might be important for the flow near the bottom, where the eddies become smaller and smaller. Further work is needed for understanding the influence

of the sampling frequency on the results of the measurements. Moreover, the size of the measuring volume of the LDV system should ne selected according to the objects of the experiment.

4.2 Distribution of depth-averaged quantities of the separating flow

After two series of sampled data have been processed on the computer, mean velocities $\bar{U}$ and $\bar{V}$, turbulence intensities u' and v', Reynolds stress $-\overline{uv}$ and turbulence energy $E = u'^2 + v'^2$ are obtained at a measuring point. In each vertical, there are three measuring points. The depth-averaged values of these qualities are calculated taking the different shapes of their vertical profiles into account. The depth-averaged values are listed in Table 4 and their distributions are depicted in fig. 8, 9, 10 and 11.

The data of depth-averaged values of mean velocity, $-\overline{uv}$ and $u'^2 + v'^2$ measured by Van Kleef (ref. 9) are also depicted in fig. 8, 10 and 11. He tested earlier the separating flow in the same flume (rough bottom), using LDV and TDA together with the 45-degrees method. In his case, U_0 was 56.0 cm/s and the corresponding Chézy coefficient was about 50 $m^{\frac{1}{2}}/s$.

In the mixing layer five measuring points were taken along several verticals and the results are listed in Table 5 and plotted in fig. 12. For comparison, the vertical distributions of turbulence quantities in the main stream are plotted in fig. 13 and listed in Table 6.

Water depths along the flume were measured in a section from A6 to F6 and the longitudinal profile is depicted in fig. 14.

In Tables and figures measuring positions are indicated in the following way. For example, A4 is the fourth vertical in section A (x = -60 cm, y = 35 cm) and B35 is the fifth measuring point in vertical 3 of section B (x = 14 cm, y = 40 cm, z = 7.2 cm), see fig. 1-b.

Although the number of measuring points is insufficient to give a complete picture of a separating turbulent flow with a free surface, several conclusions can be drawn from this measurement. Van Kleef's data are included in the discussion.

a. The flow pattern in fig. 8 shows that the reattachment occurs at about x = 1.5 m, which is 7.5 (B_0-B_1). Abbott and Kline report that when the expansion ratio is $B_1/B_0 = 1.5$ (as in the present case), the overall length of separation is about $4\ B_0 = 8(B_1-B_0)$, see ref. 1. In ref. 14 Restivo and Whitelaw, who tested turbulent flow in a duct with a symmetric sudden plane expansion, state that the length of the recirculation region is dependent upon the shape of the initial mean-velocity profile and not on the expansion ratio.

Downstream the reattachment, which is the stagnation point of velocity, the flow turns towards the straight side-wall. This turning was also observed in the experiments on unsteady separating flow, see ref. 8 and 17. Van Kleef's data show more or less the same flow pattern, except that the velocity vectors point slightly more in the -y direction.

b. Fig. 9 and 11 show that a peak of turbulent intensities and energy appears immediately downstream of the protruding corner of the expansion. The peak flattens in the direction of the flow and the locus of the peak is only slightly curved instead of following the circulating streamlines. This character of turbulent flow past an expansion has been observed by earlier workers in both vertical and plane expansions. See ref. 1, 4, 5, 7 and 12.

At $x \geq B$, the peak turbulence intensity u' reaches its maximum value ($\simeq 0.15\ U_0$). In some experiments reported in the literature (ref. 4, 5 and 7), u'_{max} is about $(0.18 \text{ to } 0.20)U_0$.

In the main stream, however, the turbulence intensities remain at the same level as in the approach flow. In this measurement u' is always larger then v' while in the case of a backward facing step in the bottom, v' may exceed u' somewhere in the recirculation region (ref. 4).

c. The separating flow has the maximum Reynolds stress in the mixing layer (fig. 10) where $\partial\overline{U}/\partial y$ is maximum. Zero Reynolds stress appears in the central part of the main stream, where $\partial\overline{U}/\partial y$ is about zero. Van Kleef's data show some anomalous distributions of $\overline{uv}$ at x = 80 cm and 120 cm, see fig. 10. A possible source of errors is the 45-degrees method, in which the Reynolds stress is obtained by subtracting the averages of readings in two directions.

d. In fig. 12 the vertical profiles of turbulence intensities u' and v' in the mixing layer are nearly uniform from section B to section F. The turbulence is mainly caused by the steep velocity-gradient $\partial\overline{U}/\partial y$ in the mixing layer, which is nearly independent of z. This is in accordance with lean and weare's conclusion: when $g^{\frac{1}{2}}/C < L/h < C^2/g$, the shear layer turbulence is dominant (ref. 10), here L is the length of the recirculation region. As opposed to the mixing layer, turbulence quantities in the main stream, where the bed-gnerated turbulence is dominant, vary linearly with z, as shown in fig. 13.

e. The weak non-uniformity of $\overline{V}$-profiles (fig. 12-b) indicates that there is no noticeable spiral flow in the mixing layer.

5. Summary and conclusion

The friction velocity in the approachflume was determined in three ways. The vertical distributions of turbulence quantities in the approach flume were obtained. The results are not conclusive. The causes may be: (1), the influence of the expansion on the water level and the velocity profiles (the testing section of velocity profiles was 72 cm upstream of the expansion section), which is difficult to account for; (2), the restriction of LDV, because a long-focus lens was required. The small angle between the laser beams produces a long measuring volume. The magnitude of recieved signals may be reduced owing to the different motions of vortices within the volume. The inconstant speed of the grating in LDV gives rise to a strong noise of about 48 Hz. The data sampled with a frequency of 100 Hz has to be filtered in order to obatin meaningful results.

The measurements of the separating turbulent flow comprised the distributions of the depth-averaged values of mean velosity and turbulence quantities in the separation region and the vertical distributions of mean velocities and turbulence quantities in the mixing layer.

The following conclusions can be drawn:

a. In a fully developed turbulent flow in shallow water, a short measuring volume of laser beams in LDV is required to measure the Reynolds stress distribution, because the vortices in the flow become smaller and smaller near the bottom. Further research is suggested to examine the influence of the size of the measuring volume on the results of the measurement.

b. In a separating turbulent flow with a signle step-expansion (expansion ratio = 1.5), the length of attachment is about 7.5 times the increase in flume width at the expansion section. After reattachment, the flow turns slightly towards the opposite side-wall.

c. The turbulence intensities u' and v' have a narrow peak in the mixing layer immediately downstream of the protruding corner. The peak values increase with x, the distance from the corner,

until a maximum is reached at $x \geq B$, where $u'_{max} \simeq 0.15\ U_0$.

d. The mixing layer turbulence gradually spreads in the direction of the flow. The mixing layer is only slightly curved rather than following the circulating streamlines.

e. Peak values of Reynolds stresses $-\overline{uv}$ also appear in the mixing layer where the velocity gradient $\partial\bar{U}/\partial y$ is maximum. There seems to be a relationship between the distribution of $\overline{uv}$ and the horizontal velocity profile.

f. The verticle distribution of turbulence intensities is more or less uniform in the mixing layer, where the source strength of turbulence is independent of the vertical coordinate. There seems to be no noticeable spiral motion in the mixing layer.

Acknowledgements

The work described here was done in the Laboratory of Fluid Mechanics, Department of Civil Engineering, Delft University of Technology. The writer is grateful to Prof. J.P.Th. Kalkwijk and Dr. C. Kranenburg for the interesting subject and many instructive discussions. Many thanks are given to other members of the Laboratory who have been very helpful concerning instrumentation, programming and typing.

References

1. Abbott, D.E. and Kline, S.J.,
Experimental investigation of subsonic turbulent flow over single and double backward facing steps.
J. Basic Engineering, Trans. ASME, Sep. 1962, p. 317.

2. Bendat, J.S. and Piersol, A.G.,
Random Data: Analysis and Measurement Procedures.
Wiley-Interscience, 1971.

3. Breusers, H.N.C.,
Lecture notes on turbulence.
IHE, 1982.

4. Etheridge, D.W. and Kemp, P.H.,
Measurements of turbulent flow downstream of a rearward facing step.
J. Fluid Mech. 1978, vol. 86, part 3, p. 545.

5. Freeman, A.R.,
Laser anemometer measurements in the recirculating region downstream of a sudden pipe expansion.
Proc. of the LDA-Symposium, Copenhagen, 1975, p. 704.

6. Hinze, J.O.,
Turbulence, 2nd. ed.,
McGraw Hill, New York, 1975.

7. Kim, J., Kline, S.J. and Johnston, J.P.,
Investigation of a reattaching turbulent shear layer: flow over a backward facing step.
Trans. ASME, J.F. Eng., 102 (1980) 3, p. 302.

8. Koppel, T.,
Experiments on unsteady separating flow in an open channel.
Internal Report no. 3-81, Laboratory of Fluid Mechanics, Department of Civil Engineering, Delft University of Technology, 1981.

9. Kleef, E.A. van,
Private communication: Measured data of a separating flow. 1981.

10. Lean, G.H. and Weare, T.H.,
Modeling two-dimensional circulating flow.
J. Hydr. Div., Proc. ASCE, vol. 105, HY1, Jan. 1979, p. 17.

11. Lynn, P.A.,
An Introduction to the Analysis and Processing of Signals.
Macmillan Press, 1973.

12. Mehta, P.R.,
Flow characteristics in two-dimensional expansions.
Proc. ASCE, J. Hydr. Div., vol. 105, HY5, May 1979, p. 501.

13. Rabiner, L.R. and Gold, B.,
Theory and Application of Digital Signal Processing.
Prentice-Hall, 1975.

14. Restivo, A. and Whitelaw, T.H.,
Turbulent characteristics of the flow downstream of a symetric plane sudden expansion.
Trans. ASME, J.F. Eng., 100 (1978) 3, p. 308.

15. TPD, Beschrijving van de Laser Doppler Snelheidsmeter,
Rapport, 1977.

16. Ven Te Chow,
Open-Channel Hydraulics.
McGraw-Hill, 1959.

17. Wang, L-X.,
Experiments on unsteady separating flow with a free surface.
Internal Report no. 7-82, Laboratory of Fluid Mechanics,
Department of Civil Engineering, Delft University of Technology, 1982.

18. Boer, S. de and Klaasman, H.
Private communication: Programmes for data processing, 1981.

19. Schlichting, H.,
Boundary-layer Theory, 6th ed.
McGraw-Hill, New York, 1968.

20. Henderson, F.M.,
Open Channel Flow.
Macmillan, New York, 1966.

Table 1. Slope of water surface J and friction velocity U_*

iterm	instrument	testing section	Δx (cm)	Δh (mm)	J $\times 10^4$	U_* (cm/s)
1	P T	II,III	100	0.25	2.50	1.01
2	P T	II,IV	200	0.71	3.55	1.27
3	P T	III,IV	100	0.46	4.60	1.48
4	WLDM	II,III	100	0.23	2.30	0.96
5	WLDM	II,IV	200	0.71	3.55	1.27
6	WLDM	III,IV	100	0.48	4.80	1.51

Table 2. $\bar{U}$-profile slope α and friction velocity U_*

Testing date	instrument	α	U_*(cm/s)
22, June, 1982	LDV, TDA	0.1849	1.48
5, July, 1982	LDV, TDA	0.1881	1.50
28, June, 1982	LDV, DAS	0.1646	1.32

Tabel 3. Values of U_* in approach flume

U_* obtained from	Instrument	U_*(cm/s)	corresponding Chézy coefficient ($m^{\frac{1}{2}}/s$
1. Water surface slope	WLDM and/or PT	1.49	42
2. $\bar{U}$-profile	LDV, TDA or LDV, DAS	1.43	44
3. Reynolds stress	LDV, DAS	1.00($\pm$ 0.1)	62

Table 4. Depth-averaged values in separating flow

vertical	mean velocity				turbulence intensity		Reynolds stress	turbulence energy
	$\bar{U}$ cm/s	$\bar{V}$ cm/s	$(\bar{U}^2+\bar{V}^2)^{\frac{1}{2}}$ cm/s	θ degrees	u' cm/s	v' cm/s	$-\overline{uv}$ cm^2/s^2	$u'^2+v'^2$ cm^2/s^2
A - 4	46.6	-2.4	46.6	-3	4.2	2.4	-0.5	26.5
- 5	54.1	-2.7	54.1	-3	4.5	2.6	-0.1	31.3
- 6	54.5	-3.0	54.6	-4	4.4	2.5	1.2	29.8
B - 1	-0.7	-0.7	1.0	-134	1.2	0.7	0.1	2.0
- 2	-1.3	-1.7	2.1	-128	1.5	1.1	-0.2	3.4
- 3	21.7	-0.6	21.7	-2	7.5	4.6	-18.6	78.0
- 4	49.7	-2.0	49.7	-2	3.9	2.4	- 0.2	23.3
- 5	58.2	-2.9	58.3	-3	3.9	2.4	0.1	25.3
- 6	56.7	-3.1	56.7	-3	4.0	2.5	1.6	25.8
C - 1	-7.2	-0.5	7.2	176	3.9	2.6	-2.6	23.5
- 2	8.8	0.0	8.8	0	6.7	5.0	-11.4	70.6
- 3	31.8	0.2	31.8	0	8.7	5.7	-24.1	107.6
- 4	49.3	-1.0	49.3	-1	4.7	3.2	0.37	35.9
- 5	57.7	-2.1	57.7	-2	4.2	2.6	-0.4	28.5
D - 1	-7.2	1.2	7.3	170	5.8	4.1	-8.3	52.4
- 2	16.8	1.3	16.	4	8.3	6.0	-20.6	105.3
- 3	34.4	1.3	34.4	2	8.3	5.7	-17.2	103.2
- 4	46.6	0.7	46.4	1	6.2	4.1	-5.4	57.7
- 5	55.5	-0.7	55.5	-1	4.3	2.9	-0.6	31.8
- 6	53.1	-1.2	53.1	-1	4.2	2.8	1.7	29.9
E - 1	3.8	0.5	3.8	8	6.7	5.0	-11.9	71.1
- 2	24.8	2.2	24.9	5	8.3	5.9	-18.3	105.5
- 3	35.4	1.8	35.5	3	7.6	5.1	-11.9	86.4
- 4	43.0	1.2	43.0	2	6.3	4.2	-6.5	58.5
- 5	51.1	0.2	51.1	0	4.8	3.3	-0.9	38.4
F - 1	12.9	-1.1	12.9	-5	5.9	4.3	-7.1	56.1
- 2	27.7	-4.6	28.0	-10	7.0	5.1	-13.1	74.5
- 3	35.4	-4.4	35.7	-7	6.8	4.8	-10.1	70.5
- 4	41.2	-5.1	41.5	-7	6.2	4.3	-8.1	58.0
- 5	48.9	-6.1	49.3	-7	5.2	3.6	-0.5	42.4
- 6	42.9	-6.7	43.4	-9	4.9	3.1	2.4	35.1

Table 5. Vertical distributions in mixing layer

point	mean velocity		turbulence intensity		Reynolds stress	turbulence energy
	$\bar{U}$ cm/s	$\bar{V}$ cm/s	u' cm/s	v' cm/s	$-\overline{uv}$ cm^2/s^2	$u'^2+v'^2$ cm^2/s^2
B-3-1	19.6	-1.3	8.0	4.4	-19.3	83.4
-2	20.1	-1.3	7.7	5.0	-21.5	84.8
-3	22.1	-0.9	7.9	4.9	-21.1	86.0
-4	23.6	-0.7	7.6	4.8	-19.9	80.6
-5	24.7	0.1	6.8	4.6	-18.0	66.9
C-3-1	32.4	1.1	8.0	5.5	-15.4	95.1
-2	33.3	0.2	8.7	5.8	-26.3	109.3
-3	33.0	-0.2	9.3	5.9	-32.3	122.1
-4	33.4	-0.4	9.2	5.7	-31.8	118.2
-5	33.0	-0.1	8.7	5.6	-24.7	106.6
D-3-1	32.7	1.7	8.4	5.6	-10.0	101.6
-2	36.7	2.1	8.0	5.8	-15.8	97.7
-3	38.8	1.8	7.6	5.6	-19.2	89.4
-4	39.4	1.9	8.5	5.7	-27.0	105.8
-5	35.1	0.7	8.7	5.9	-20,9	110.1
E-3-1	30.1	1.1	8.5	5.7	-11.1	105.2
-2	34.9	2.6	7.8	5.3	-6.1	88.5
-3	39.5	3.1	6.6	4.6	-7.6	65.1
-4	40.8	2.7	6.3	4.8	-10.8	62.2
-5	38.2	1.4	7.5	5.0	-15.5	80.6
F-3-1	30.5	-5.6	7.4	5.5	-10.6	85.7
-2	33.7	-4.3	7.7	5.1	-9.4	94.1
-3	37.7	-4.0	6.6	4.6	-8.2	65.1
-4	40.2	-3.7	5.8	4.4	-8.6	52.7
-5	39.7	-4.4	6.5	4.5	-10.8	62.4

Table 6. Vertical distributions in main stream

point	mean velocity		turbulence intensity		Reynolds stress	turbulence energy
	$\bar{U}$ cm/s	$\bar{V}$ cm/s	u' cm/s	v' cm/s	$-\overline{uv}$ cm^2/s^2	$u'^2+v'^2$ cm^2/s^2
B-5-1	51.1	-2.4	5.8	3.4	1.1	45.5
-3	61.0	-2.8	4.2	2.5	-0.2	23.8
-5	66.5	-3.6	2.2	1.6	-0.7	7.5
C-5-1	50.2	-1.3	6.2	3.5	-0.0	51.5
-3	60.0	-2.1	4.6	2.6	-0.3	27.7
-5	65.9	-2.8	2.4	1.8	-0.8	8.7
D-5-1	48.2	0.1	6.5	4.0	-0.3	58.0
-3	58.2	-0.5	4.8	3.0	-0.6	32.2
-5	63.0	-1.5	2.5	2.1	-0.9	10.5
E-5-1	42.7	0.6	6.7	4.5	-1.0	65.1
-3	52.7	0.5	5.4	3.7	-0.2	42.1
-5	59.1	-0.3	3.2	2.4	-1.2	16.0
F-5-1	41.3	-6.4	6.5	4.6	0.5	63.4
-3	50.3	-6.1	5.8	3.9	0.0	48.5
-5	56.4	-6.4	3.9	2.8	-1.6	23.5

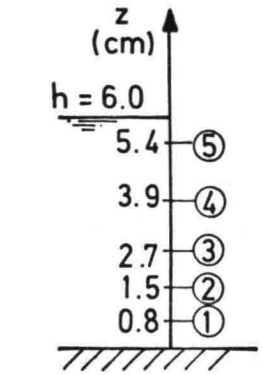

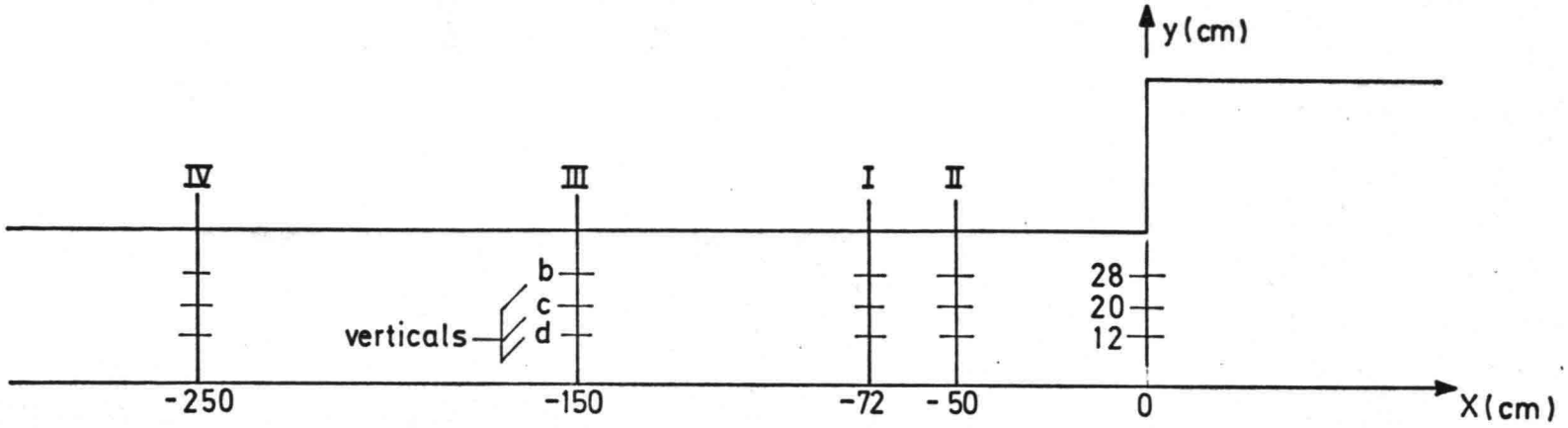

(a) in the approach flume

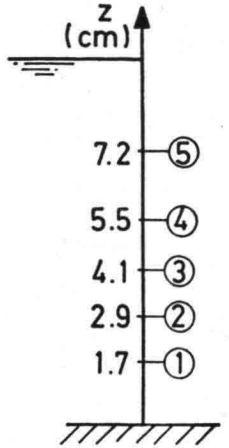

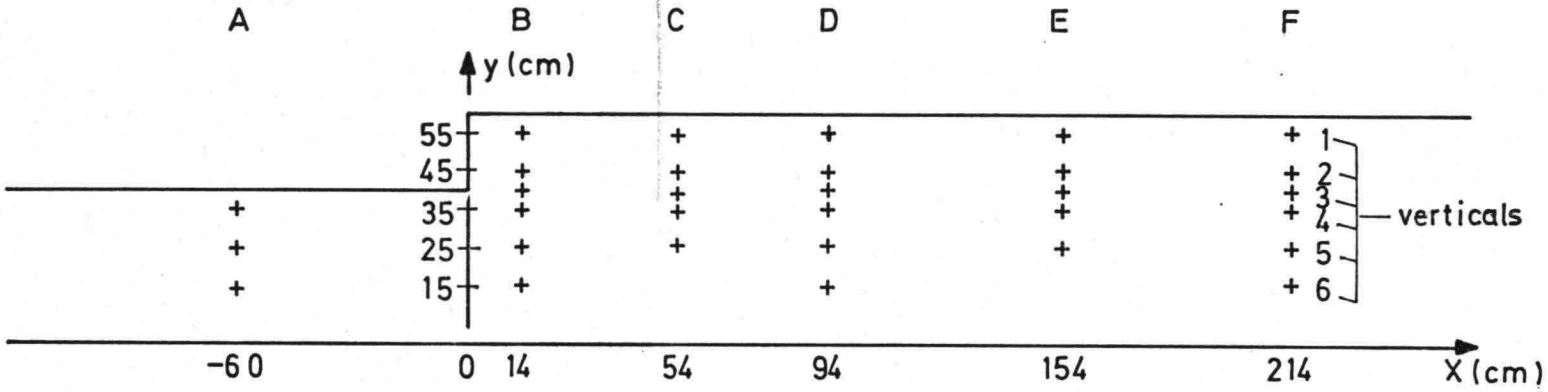

(b) in the expanding flume

Fig. 1. Schemes of measurements

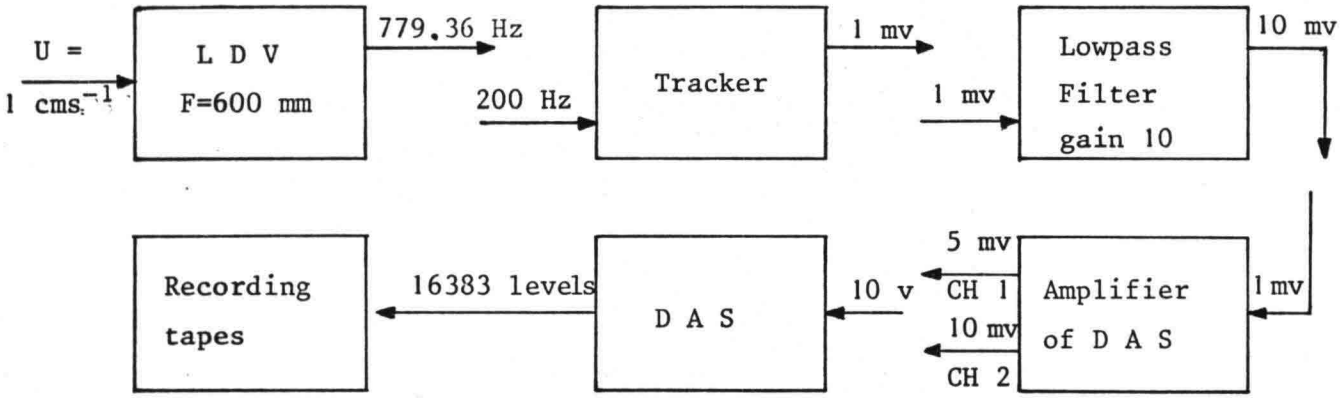

Fig. 2 Block-scheme of signal transformation

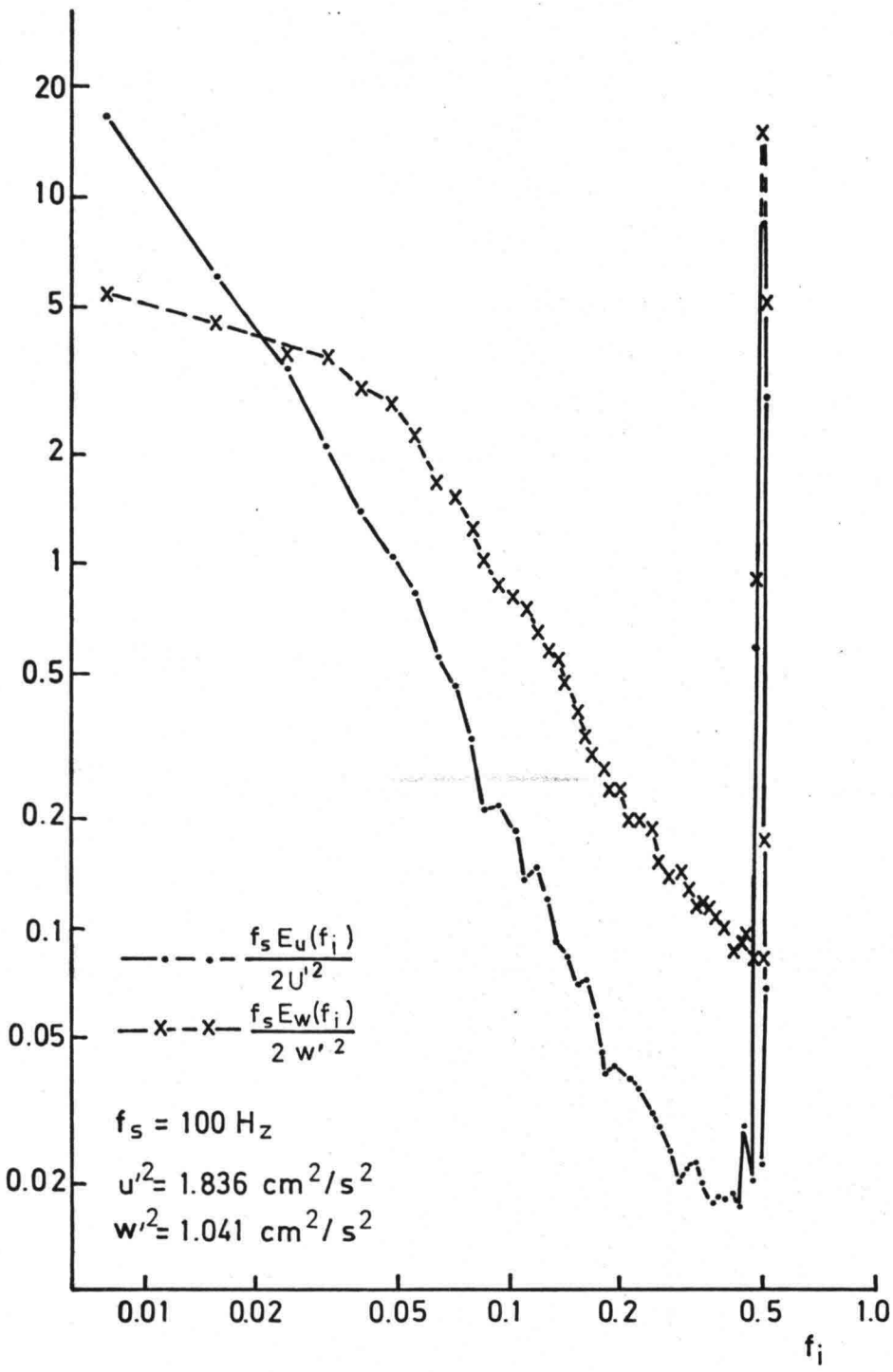

Fig. 3. Non-dimensional spectral distribution of E_u and E_w at point Ib3 (x = 72 cm, y = 28 cm, z = 2.7 cm)

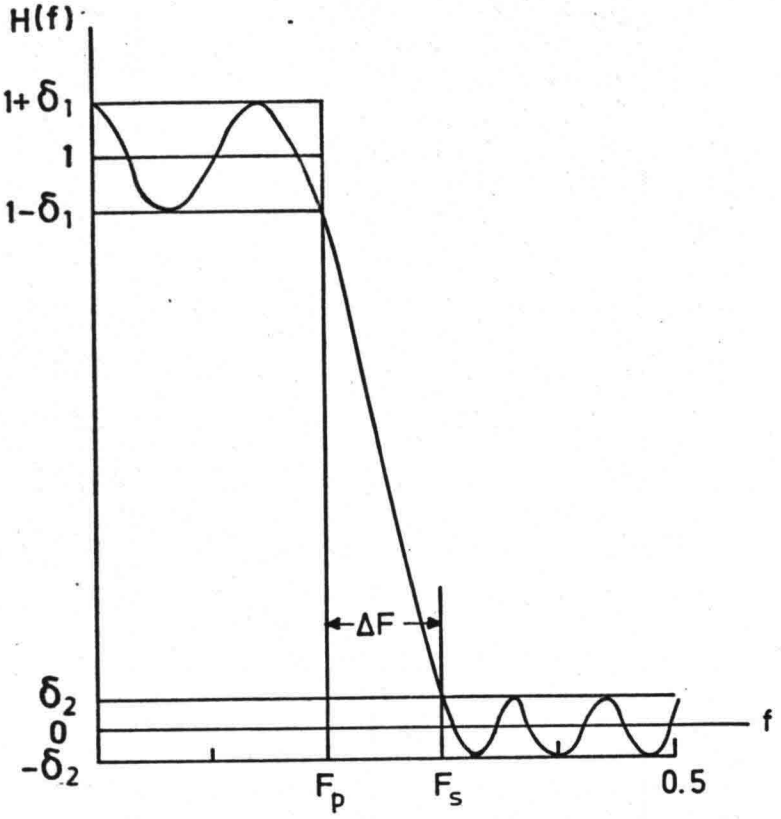

Fig. 4. Frequency response of an optimal lowpass filter

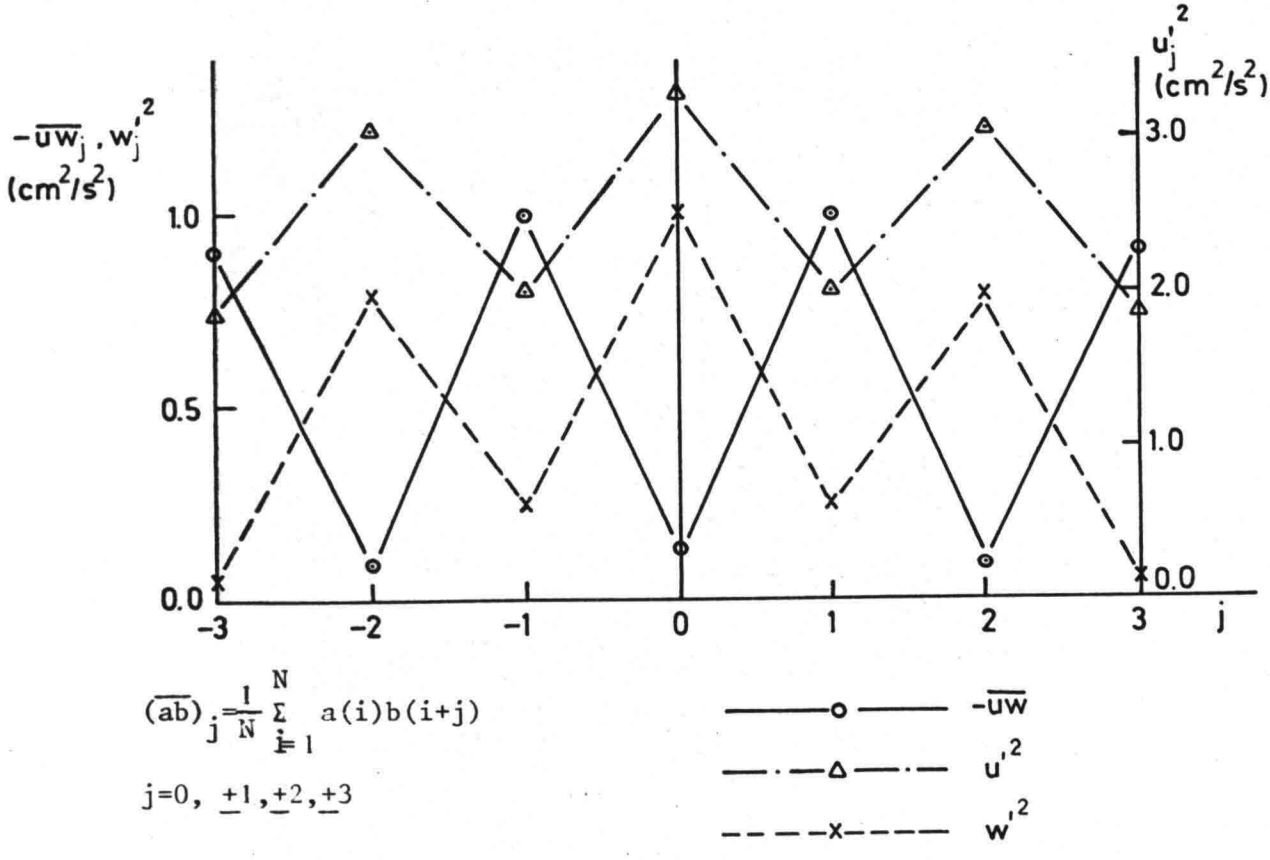

Fig. 5. Calculated turbulence quentities, oscillating with shifted steps at point Ib3

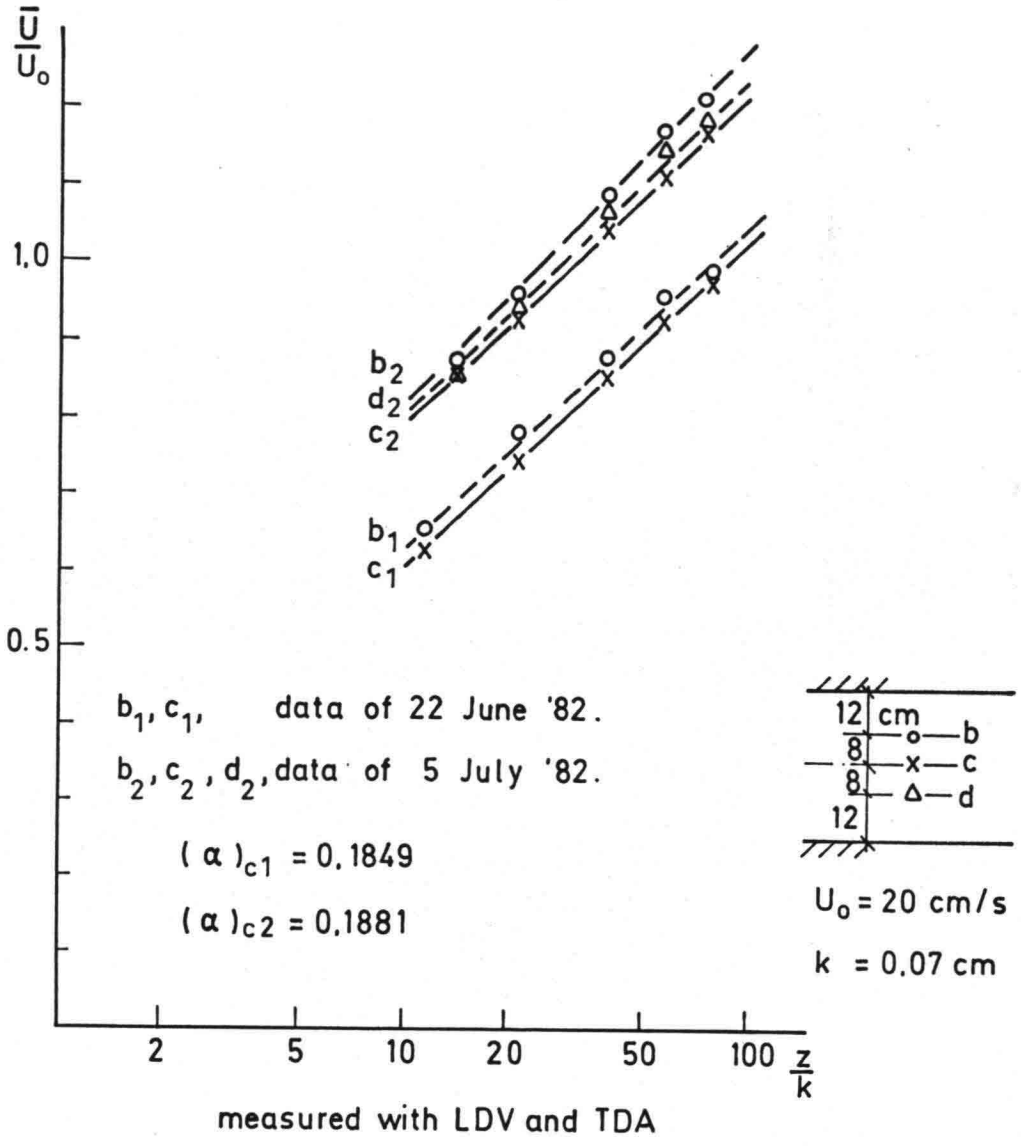

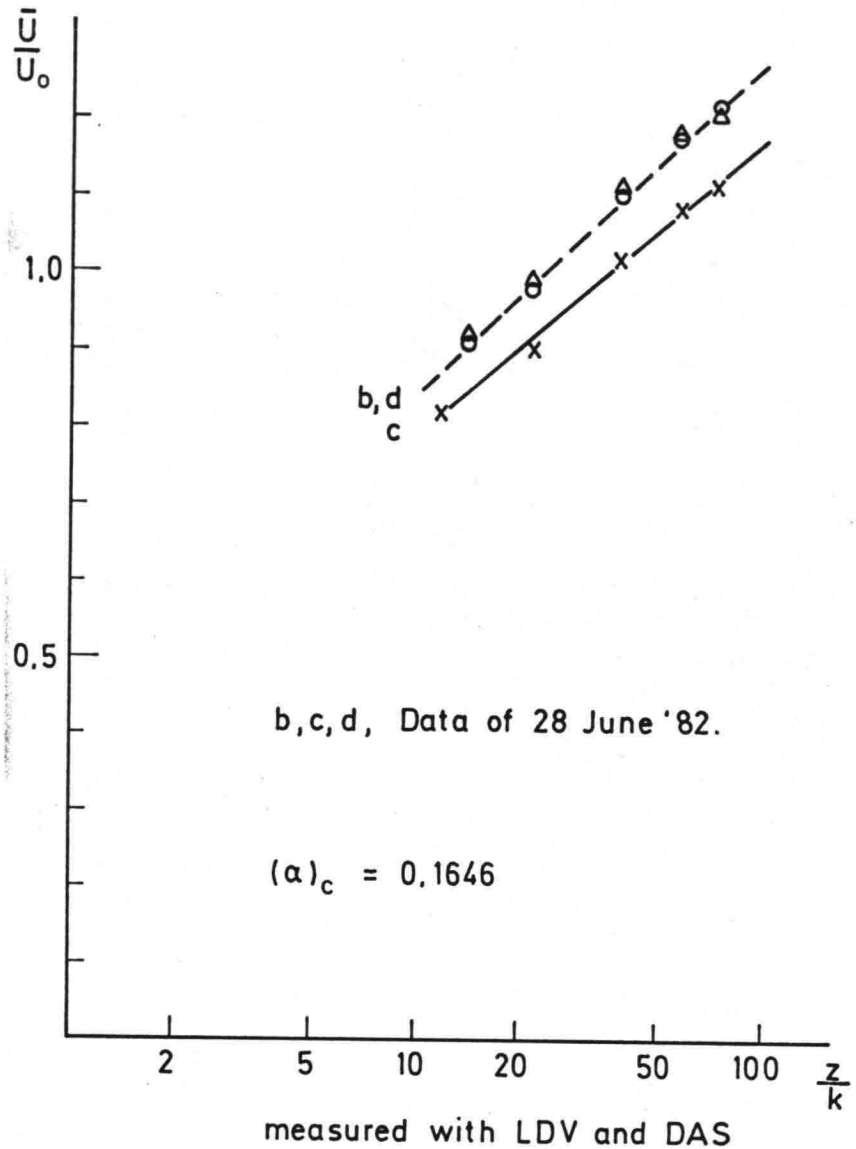

Fig. 6. Velocity profiles in the approach flume

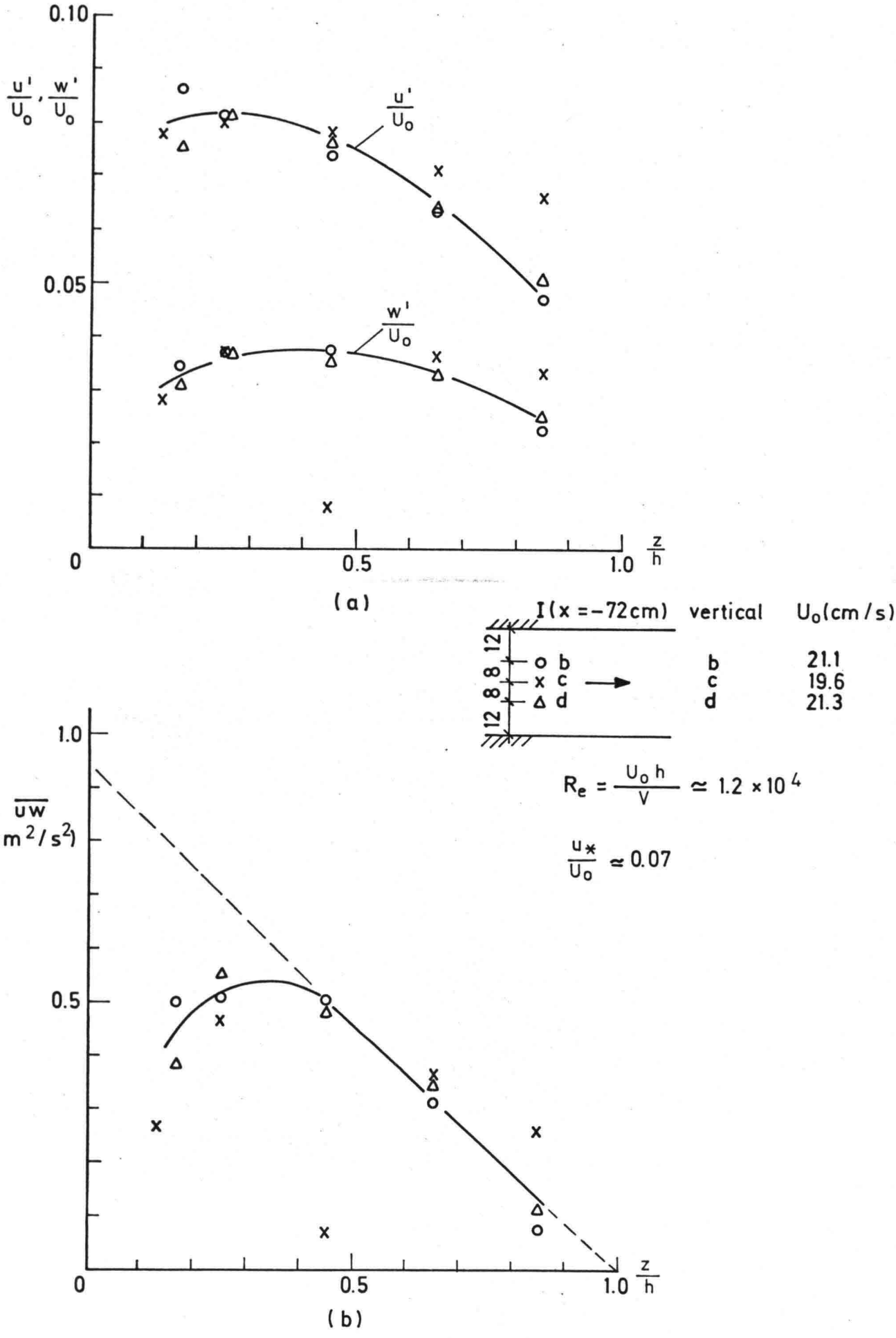

Fig. 7. Vertical destributions of turbulence quantities in the approach flume

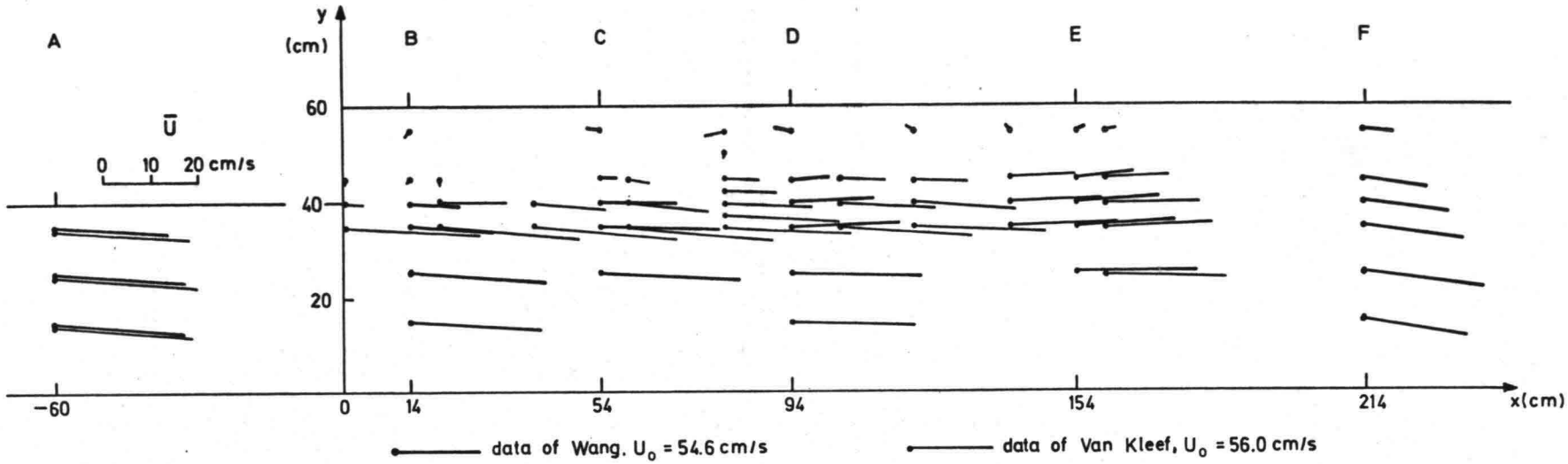

Fig. 8. Flow-pattern in the expanding flume with a rough bottom

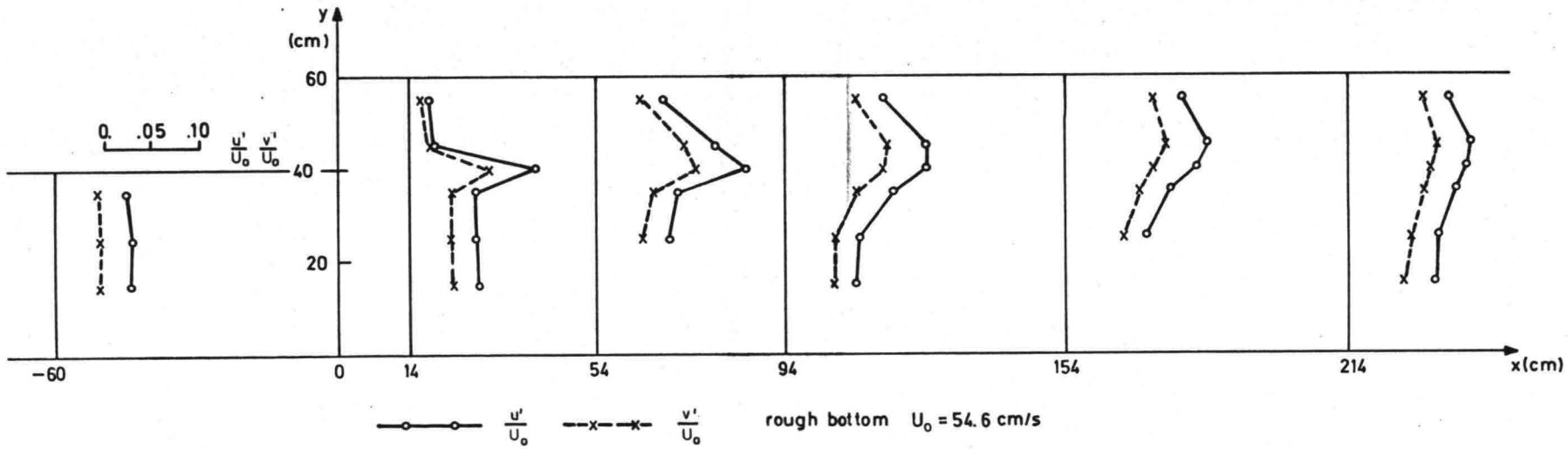

Fig. 9. Distribution of depth-averaged u' and v', rough bottom

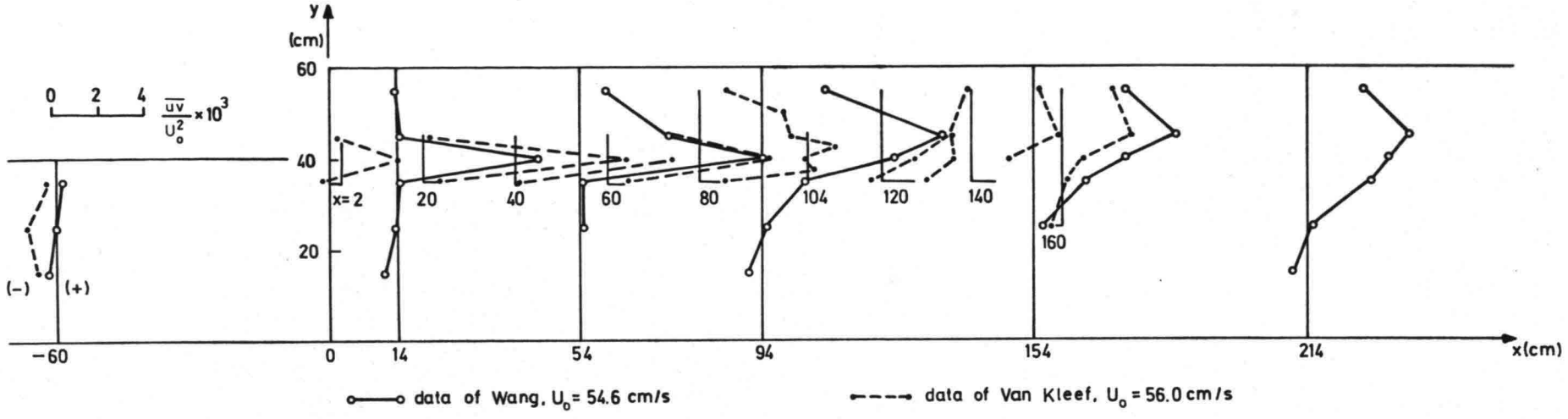

Fig. 10. Distribution of depth-averaged $\overline{uv}$, rough bottom

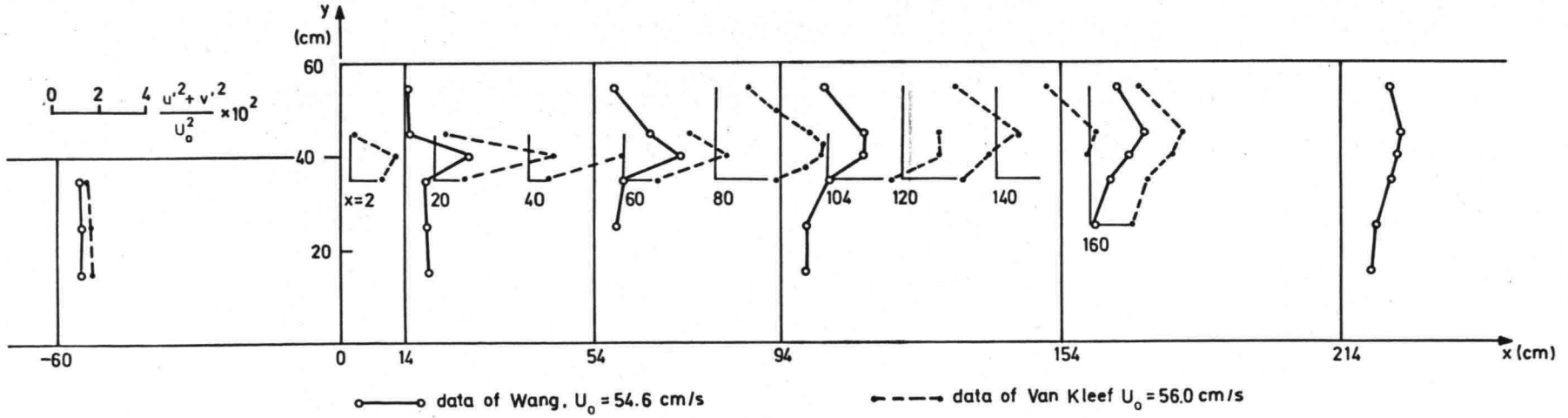

Fig. 11. Distribution of depth-averaged $(u'^2 + v'^2)$, rough bottom

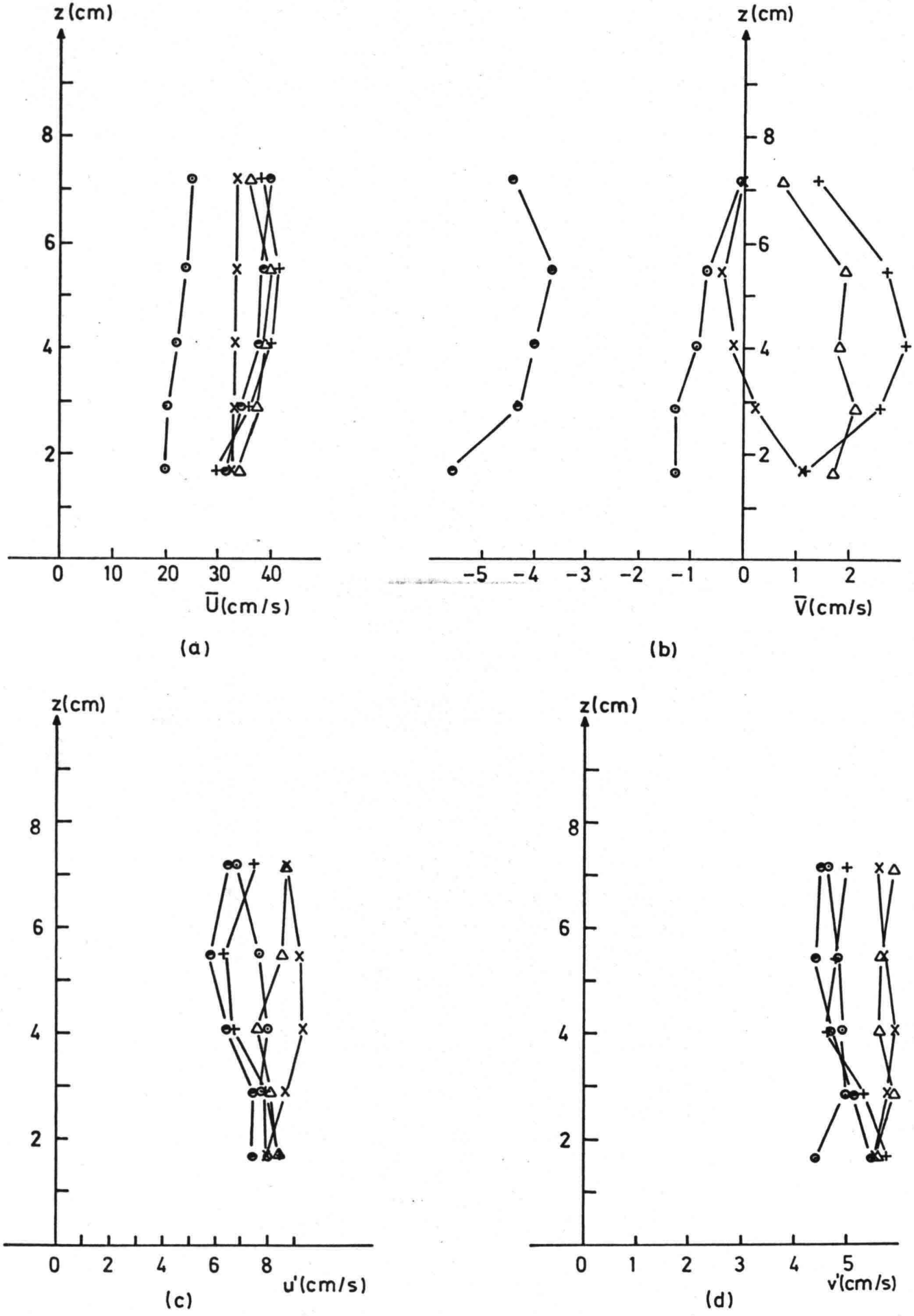

Fig. 12. Vertical distributions of $\bar{U}$,$\bar{V}$, u',v', $-\overline{uv}$ and $u'^2 + v'^2$ in the mixing layer

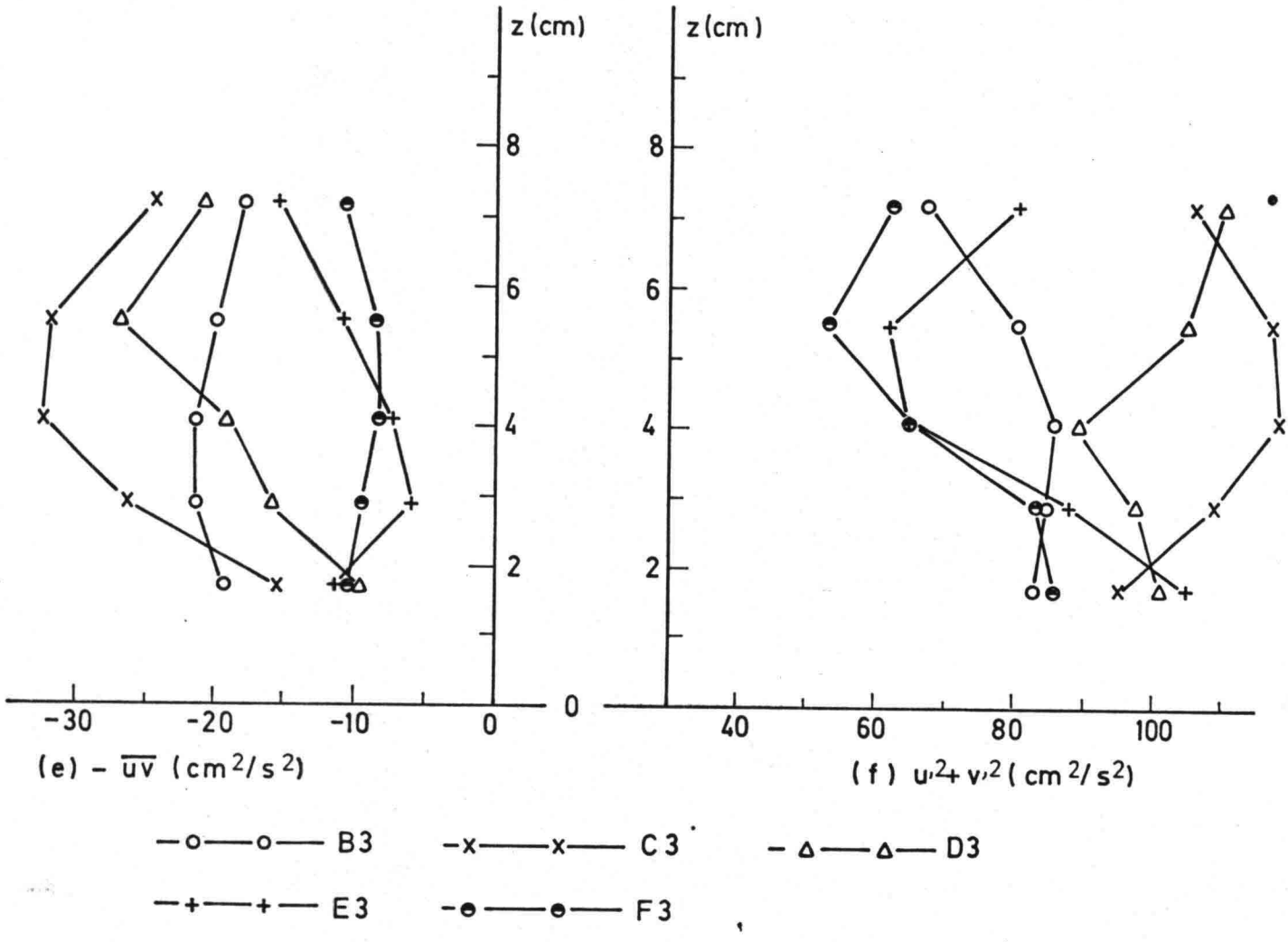

Fig. 12. (continued)

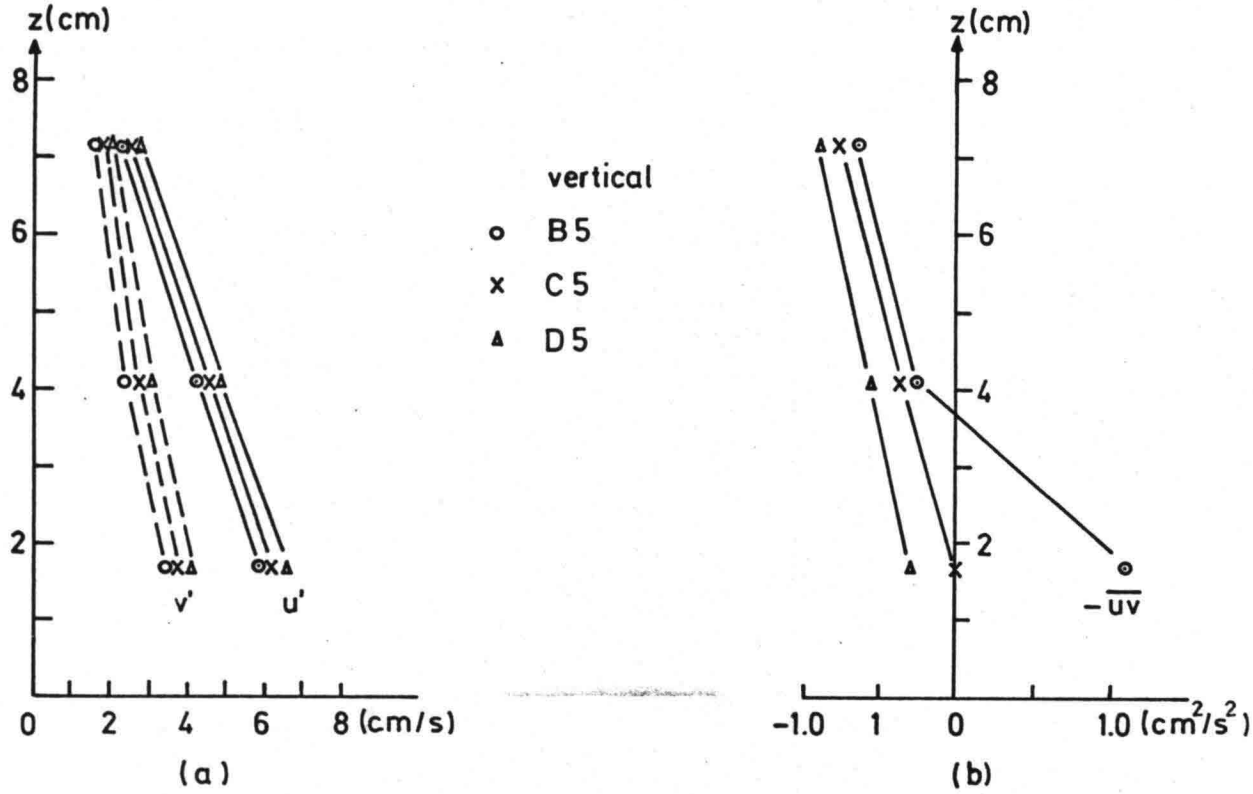

Fig. 13. Vertical distributions of u',v' and $-\overline{uv}$ in the main stream

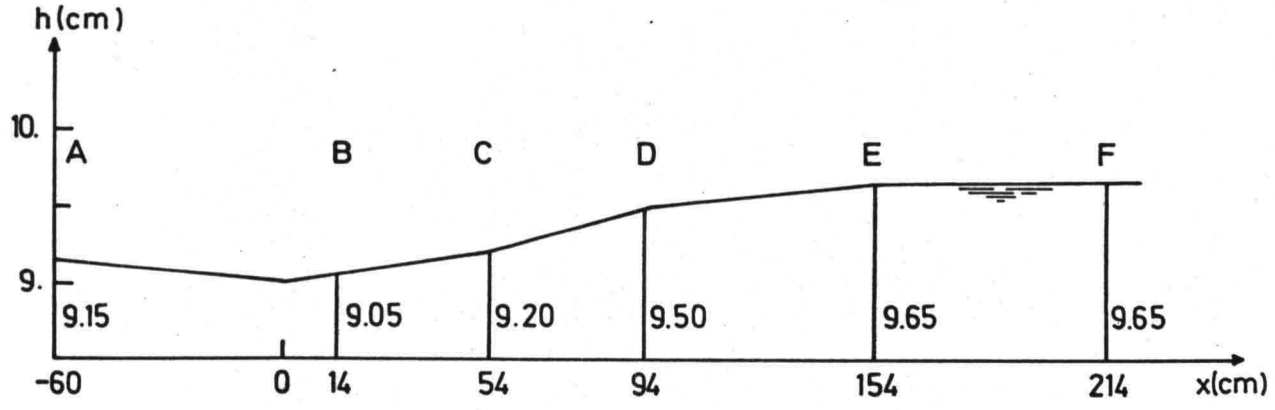

Fig. 14. Water level profile, in the section from A6 to F6